Respiratory Gating for 3-Dimensional PET of the Thorax: Feasibility and Initial Results

Luc Boucher, MD; Serge Rodrigue; Roger Lecomte, PhD; and François Bénard, MD

Metabolic and Functional Imaging Center, Clinical Research Center, Centre Hospitalier Universitaire de Sherbrooke, Sherbrooke, Quebec, Canada

Respiratory motion may reduce the sensitivity of ^{18}F-FDG PET for the detection of small pulmonary nodules close to the base of the lungs. This motion also interferes with attempts to use fused PET/CT images through software or combined PET/CT devices. This study was undertaken to assess the feasibility of respiratory gating for PET of the chest and the impact of respiratory motion on quantitative analysis. **Methods:** Ten healthy subjects were enrolled in this study. Three-dimensional studies were acquired with 8 gates per respiratory cycle on a commercial PET scanner with a temperature-sensitive respiratory gating device built in-house. All scans were obtained over 42 cm of body length with 3 bed positions of 10 min each after injection of ^{18}F-FDG at 4.5 MBq/kg. The reconstructed images were assembled to produce gated whole-body volumes and maximum-intensity projections. The amplitude of respiratory motion of the kidneys (as a surrogate for diaphragmatic incursion) as well as the apex of the heart was measured in the coronal plane. Phantom studies were acquired to simulate the impact of respiratory motion on quantitative uptake measurements. **Results:** The respiratory gating device produced a consistent, reliable trigger signal. All acquisitions were successful and produced reconstructed volumes with excellent image quality. Mean ± SD motion amplitude and maximal motion amplitude values were 6.7 ± 3.0 and 11.9 mm for the heart, 12.0 ± 3.7 and 18.8 mm for the right kidney, and 11.1 ± 4.8 and 17.1 mm for the left kidney, respectively. In phantom studies, the standardized uptake value for a 1-mL lesion was underestimated by 30% and 48% for the average and maximal respiratory motion values, respectively. **Conclusion:** Respiratory gating of PET of the thorax and upper abdomen is a practical and feasible approach that may improve the detection of small pulmonary nodules. Further work is planned to assess prospectively the diagnostic accuracy of this new method.

Key Words: motion correction; respiratory gating; ^{18}F-FDG; PET

J Nucl Med 2004; 45:214–219

PET technology has improved significantly in the last 20 y. The effectiveness of PET for the evaluation of patients with a solitary lung nodule or documented bronchogenic carcinoma is no longer in doubt (*1–3*). Despite some shortcomings, several studies have demonstrated the utility of static ^{18}F-FDG uptake values, such as the standardized uptake value (SUV), for distinguishing benign from malignant pulmonary nodules, and this parameter can be used to monitor tumor metabolic changes after treatment (*4*). However, the SUV can be influenced by imaging techniques or individual patient characteristics, such as weight (*5–7*), plasma glucose level (*8,9*), or delay after ^{18}F-FDG injection (*10*). It is well known that respiratory motion can produce artifacts on CT (*11–13*) and MRI (*14,15*), and this motion certainly has an impact on thoracic PET studies (*16*) and on SUV measurements, particularly for small lesions and those near the base of the lungs. The qualitative aspect of the heart, diaphragmatic muscles, liver, spleen, and pancreas is also most likely influenced by respiratory motion. With the development of new combined PET/CT devices, the impact of respiratory motion during PET imaging acquires an even greater importance, as it interferes with coregistration of the metabolic data on the anatomic images. The objectives of this study were to demonstrate the feasibility of respiratory gating of PET of the chest and upper abdomen and to quantify the impact of respiratory motion on the underestimation of lesion activity.

MATERIALS AND METHODS

Healthy Subjects

A total of 10 healthy subjects (5 female and 5 male, 31.3 ± 12.7 y old [mean ± SD]) were enrolled in this study. All subjects had fasted for at least 6 h before PET imaging. A peripheral venous access was installed, and the capillary glucose level was measured before ^{18}F-FDG injection with a portable glucometer (Accusoft Advantage; Roche Diagnostics). The capillary glucose level was normal in each subject (mean ± SD, 4.3 ± 0.7 mmol/L).

^{18}F was produced with a 19-MeV TR PET Cyclotron (Ebco Technologies Inc.) by use of an ^{18}O-water target. ^{18}F-FDG was produced with an automated synthesis module by use of nucleophilic substitution, modified from the synthesis technique previously described by Hamacher et al. (*17*).

For respiratory gating, a temperature-sensitive device was built in-house (Fig. 1). A sensitive thermistor was connected to a discriminator, producing a 5-V pulse and a visual signal (light-emitting diode pulse) whenever the exhaled temperature rose above a value selected with a variable-resistance dial to produce a consistent signal at the beginning of inspiration. The thermistor

Received Apr. 25, 2003; revision accepted Oct. 23, 2003.

For correspondence or reprints contact: François Bénard, MD, Metabolic and Functional Imaging Center, Clinical Research Center, CHUS/Hôpital Fleurimont, 3001 12th Ave. Nord, Sherbrooke, Quebec, Canada J1H 5N4.

E-mail: francois.benard@usherbrooke.ca

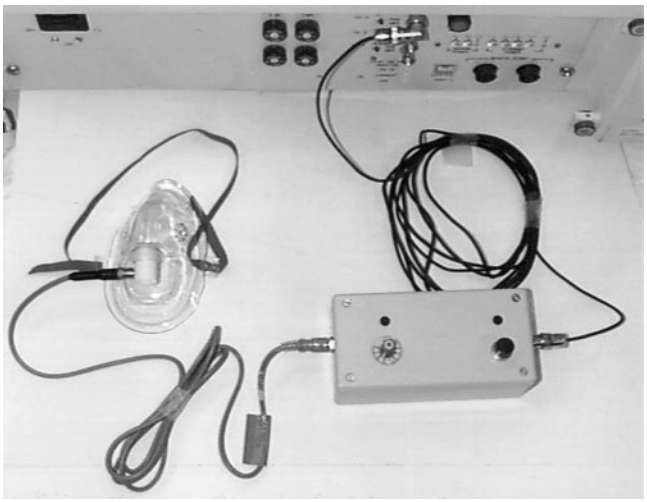

FIGURE 1. Respiratory gating device built to trigger gated acquisition at the start of each breathing cycle. A high-sensitivity thermistor was installed at the inlet of a conventional disposable oxygen face mask. This thermistor was connected to a simple circuit equipped with a discriminator and a variable-resistance dial, powered by 5 V with AA batteries. The output of this circuit was fed to the 5-V input of the PET scanner.

was inserted into the entry of a transparent breathing mask covering the nose and the mouth of the subjects, so that air exchanges circulated around the thermistor. At 10 min before PET acquisition, the breathing mask was placed on the subjects, allowing the thermistor temperature to be adjusted to the subject's exhaled air. It was possible to regulate the respiratory pulse emission with the variable-resistance dial to modify the temperature threshold necessary to give a signal.

The subjects were imaged with a full-ring dedicated PET system (ECAT Exact HR+; CPS/Siemens). All subjects were injected with ^{18}F-FDG at 4.5 MBq/kg (211–311 MBq). The PET study was obtained without septa (3-dimensional [3D] mode) at 60 min after ^{18}F-FDG administration. The scans were acquired with 8 gates per respiratory cycle by use of the electrocardiographic gating acquisition software supplied by the manufacturer. All respiratory signals sent by the gating device that were situated outside a window of 4–30 respirations per minute were automatically rejected during acquisition. Gated emission scans were obtained over 42 cm of body length, including the thorax and upper abdomen, with 3 bed positions of 10 min each. Transmission scans were obtained after injection with the same bed positions of 3 min each. The transmission acquisition was not gated with respiration.

The gated emission data were reconstructed by use of Fourier rebinning and the ordered-subset expectation maximization algorithm with 2 iterations and 16 subsets. Postfiltering was applied with a gaussian filter for a final reconstructed resolution of 10 mm. The individual gated bed positions were sorted by software written in-house to simulate 8 separate whole-body studies and assembled by use of ECAT software (CTI) to produce complete volumes (neck to upper abdomen) corresponding to each gate of the respiratory cycle. Three-dimensional maximum-intensity projections also were produced from each of these gated volumes. These studies were combined to obtain a gated whole-body file and a gated projection file. Thus, it was possible to visualize the respiratory motion-gated planes and the gated 3D projections in cine mode by use of the standard viewers provided by the scanner manufacturer.

The coronal respiratory motion-gated planes were analyzed with a cine viewer. The amplitude of the respiratory motion of the kidneys was used as a surrogate for diaphragmatic excursion. Cardiac motion was measured at the apex of the heart. The measurements were taken on the coronal plane showing the maximal difference throughout the respiratory cycle.

Phantom Studies

An elliptic phantom (model ECT/ELP/P; Data Spectrum Corp.) filled with water was acquired to evaluate the impact of respiratory motion on lesion quantification. To simulate spheric lesions, 5 hollow spheres (volumes of 1.2, 2.0, 5.5, 11.5, and 19.4 mL) filled with a solution of ^{18}F at 427 kBq/mL were placed in the middle of the phantom. Eight emission and transmission frames were acquired. The scanner table was moved a few millimeters between each frame (Table 1) to simulate the vertical motion encountered in a typical respiratory motion-gated study. Only the vertical motion (as measured in the healthy subjects) was applied to the phantom. Lateral and anteroposterior respiratory motion components were not considered in these phantom studies. The emission acquisition times for the average and maximal respiratory motion phantom studies were 600 and 240 s, respectively. The transmission time for the 2 phantom studies was 300 s at each bed position.

The maximal respiratory motion phantom represented the motion measured between each set of gates for the subject showing the largest respiratory incursion (Table 1). The average respiratory motion phantom represented the average amplitude measured in millimeters between 2 gates for the 10 healthy subjects after the gates were realigned so that the maximal amplitude always occurred in the same gate. This step was necessary because the largest motion did not occur exactly in the same gate from one subject to another, and simply averaging the values would have underestimated the true extent of respiratory motion. This situation was attributable to normal variations in respiratory rates between subjects. Thus, the highest displacement values in Table 1 were not observed in the same gates for the average and maximal respiratory motion phantoms.

The emission data were reconstructed by use of Fourier rebinning and the ordered-subset expectation maximization algorithm with 2 iterations and 16 subsets. Postfiltering was applied with a gaussian filter for a final reconstructed resolution of 7 mm, and a zoom factor of 1.5 was applied. To obtain a "nongated" study, the emission and transmission sinograms of the 8 frames were summed, and a single composite image was reconstructed from the data for comparison with the first frame of the acquisition (without motion) as a reference study. The total and maximal activity concentrations (Bq/mL) of the nongated and reference studies

TABLE 1
Bed Movement Between Simulated Gates Used for Phantom Acquisition

Respiratory motion	Movement (mm) for the following bed position:							
	1	2	3	4	5	6	7	8
Average	0	2.2	0.8	1.4	1.6	6.0	0.1	0.3
Maximal	0	3.4	8.6	1.8	1.7	1.6	1.7	0.1

were measured for each sphere by use of the region-of-interest (ROI) tool without correction for partial-volume effects. The mean activity concentration for a sphere also was measured with the same tool. The ROIs used were spherical, with a diameter corresponding exactly to the known diameter of the spheres used in the phantom experiments. Each ROI was applied from the top to the base of each sphere visualized in the phantom acquisitions.

Data Analysis

The maximal motion for the apex of the heart and the right and left kidneys was calculated and expressed as mean ± SD. The activity concentrations measured for the phantom spheres were compared, and the differences were calculated and expressed as a percentage of the value for a still frame of the same object.

RESULTS

All healthy subjects tolerated the gating device well for the duration of the PET study without any spontaneous complaint about its use. There were no problems in adjusting the variable resistance to obtain a regular respiratory pulse signal for all of the subjects at the beginning of the study. It was nevertheless important to monitor the respiratory gating signal to ensure that there were no shifts in the thermistor temperature outside the initial setting, as minor adjustments of the variable-resistance setting occasionally were necessary during acquisition. However, these adjustments were infrequent.

The resulting gated images were all of good quality and suitable for interpretation (Fig. 2). There were no contour indentations or streaks ("stitching lines") at the bed junctions in the reconstructed images. This finding confirmed the constancy of the signal sent by the temperature-sensitive device throughout the respiratory cycle and over the acquisition duration. If seen, such artifacts could have been related to an inconsistency of the gating signal. For example, if the beginning of the inspiration were located in frame 1 of the first bed and in frame 4 of the second bed, then the body contours would not match. Visualization of the studies in cine mode also confirmed that the bed positions were well aligned and timed properly throughout the respiratory cycle. Because the transmission scan was not gated, all of the gates were corrected with a nongated transmission study. For this reason, it was difficult to distinguish clearly the limits of the base of the lungs as well as the diaphragmatic surface of the liver and the spleen.

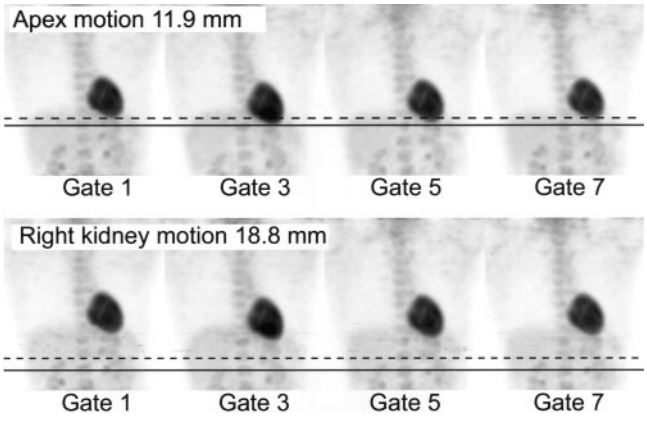

FIGURE 2. Respiratory gating of 3D projections of the thorax acquired with the respiratory gating device. The motion of the heart (upper panel) and the right kidney (lower panel) is shown. The dotted line represents the initial position of these organs at the start of the breathing cycle; the solid line represents the maximal vertical amplitude of the respiratory motion.

For an adequate estimation of the amplitude motion induced by respiration in these organs, the measurements were obtained for the apex of the heart and the 2 kidneys. Because the subjects had been fasting and were not prepared for a cardiac ^{18}F-FDG PET study, myocardial uptake was variable. For this reason, the heart was not visible in 2 subjects.

Mean ± SD and maximal motion amplitude values for the heart were 6.7 ± 0.3 and 11.9 mm for the 8 subjects with cardiac uptake of ^{18}F-FDG. These values were 12.0 ± 3.7 and 18.8 mm for the right kidney and 11.1 ± 4.8 and 17.1 for the left kidney. The right kidney was not seen clearly in 2 subjects (there was insufficient urinary activity in the cortex, the calyx, or the renal pelvis to obtain an accurate measurement), and the left kidney was not seen in 1 subject for the same reason. These results are summarized in Table 2.

The results obtained with the average motion phantom show that the average and maximal activity concentrations in the spheres were significantly underestimated. This underestimation was inversely related to the sphere volume. For a 1.2-mL sphere, the maximal activity concentration was underestimated by 41% and the average activity concentration was underestimated by 40%. The trend was similar with the maximal motion phantom. With this phantom, the maximal and average activity concentrations were underestimated by 44.8% for the 1.2-mL sphere. The results of the phantom studies are summarized in Table 3 and Figure 3.

DISCUSSION

Respiratory motion-induced artifacts have been overcome in SPECT (*18*), CT, CT-guided needle biopsy, and MRI by use of different modalities of respiratory gating, such as spirometry (*19*,*20*), impedance plethysmography, interruption of an infrared beam (*21*), and a thoracic band sensitive to stretching. In this study, we used a device that was sensitive to minimal temperature changes and that was fixed to a conventional transparent breathing mask. This device has several advantages: It is easily built, it has a very low cost, and there are no systems surrounding patients to impair breathing. This device probably can be used for the majority of patients evaluated with PET for a thoracic or an abdominal lesion, except perhaps for patients with oxygen dependency, because the external air flow could confuse the temperature probe. The electrical pulses given by the device were designed to be similar to those obtained with standard electrocardiographic gating devices. Thus, the signal was used directly with standard gating software. A visual signal

TABLE 2
Organ Motion Observed Throughout Respiratory Cycle

Patient	Sex	Age (y)	Motion (mm) observed for: Apex of heart	Kidney: Right	Kidney: Left
1	M	32	11.9	18.8	17.1
2	M	22	8.6	13.7	13.7
3	M	23	5.1	8.6	3.5
4	M	47	3.4		
5	M	26	5.2		5.2
6	F	20	6.8	10.3	12.0
7	F	20	10.3	13.7	15.5
8	F	49		13.7	12.1
9	F	51	5.1	6.9	6.9
10	F	23	3.5	10.3	13.7
Mean		31.3	6.7	12.0	11.1
SD		12.7	3.0	3.7	4.8

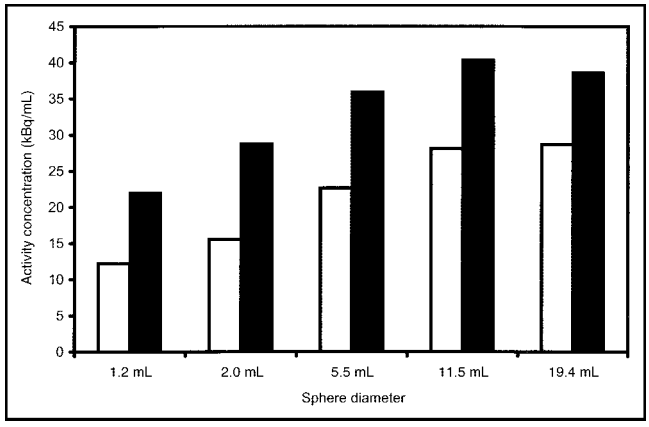

FIGURE 3. Bar graph showing the maximal activity concentrations measured in the spheres in a phantom study simulating the subject with the largest respiratory amplitude (white bars) in comparison with the same measurements obtained without simulated respiratory motion (black bars).

activated at the same time as the scanner trigger signal allowed technologists to confirm that a stable trigger was emitted at the beginning of each inspiration, and the trigger could be adjusted manually during the study. It was important to monitor the signal emitted by the device throughout the entire PET study, as it was occasionally necessary to adjust the temperature threshold to maintain a consistent signal throughout the acquisition. This requirement did not interrupt the acquisition of any study but created an additional burden on technologists during PET acquisition. These adjustments could slightly shift data in each bin during acquisition. Fortunately, they were rarely needed during the subject studies. We believe that the need for these adjustments was related to a progressive warming of the respiratory mask and device when a study was started too soon after the subject was situated on the table bed with a variable-resistance setting close to the limit of the signal release. This problem could be corrected by letting subjects rest longer to stabilize the device before initiating the acquisition.

TABLE 3
Activity Concentration Underestimation Resulting from Respiratory Motion in Phantom Studies

SUV	Sphere volume (mL)	% Activity concentration underestimation with the following motion phantom: Average	Maximal
Maximum	19.4	21.1	25.8
	11.5	23.5	30.5
	5.5	27.8	37.2
	2.0	32.5	46.1
	1.2	41.0	44.8
Mean	19.4	23.5	32.8
	11.5	24.2	35.1
	5.5	33.6	42.2
	2.0	33.1	44.8
	1.2	40.0	44.8

We limited our acquisitions to 3 bed positions and 42 cm of body length over the thorax and upper abdomen to maintain the study duration at a reasonable length. We used a 3D acquisition to obtain sufficient counts in each gate of the PET study, as 2D images likely would have been count starved because of the low sensitivity of this acquisition mode. Because of the setup time of each gated acquisition and the length of the transmission scan, the entire study took approximately 1 h. With optimized software, the overhead could be reduced substantially. Our acquisition protocol produced 24 sinograms for coverage of the chest, necessitating long reconstruction times and large storage requirements. The total data storage requirement for a gated study of the chest (sinograms plus final reconstructed data), excluding intermediate reconstruction files, was 541 megabytes compared to the 66 megabytes needed for an equivalent nongated 3D study. New computers are able to manage these additional computing requirements easily.

Semiquantitative evaluation of tumor metabolism with the SUV is used widely to assess pulmonary nodules and quantify tumor response to therapy. It has been shown that the SUV is overestimated in large patients if ^{18}F-FDG uptake is normalized with the actual patient weight (*5–7*). SUV normalization also can be done with the ideal body weight, lean body mass, or body surface area to reduce this effect (*22*). Other factors, such as the time interval after injection, plasma glucose level, and the size of the lesion, can also have significant effects on image quantification (*23*). All of these factors can interfere with tumor glucose metabolism quantification but often can be controlled or corrected to obtain valuable results.

The evaluation of lung lesions situated close the base of the lungs presents an additional challenge. It has been shown that normal lung uptake is higher in the lower lung

field than in the upper and middle lung fields (*24*). Miyauchi and Wahl (*24*) proposed that this normal variation of background activity could contribute occasionally to a lower level of detection of small lesions near the base of the lungs. Another problem is respiratory motion of the lungs and thoracic wall during PET emission and transmission acquisition. The influence of this motion on qualitative and quantitative aspects of PET studies was described previously for animals in cardiac (*25*) or pulmonary (*26*,*27*) investigations. Our phantom studies suggest that SUV measurements are underestimated by 21%–45% because of respiratory blurring, depending on the lesion size. Obviously, given that only the vertical motion was simulated in our investigation, these values represent a best-case scenario. Real respiratory blurring is significantly more complex, with additional anteroposterior and lateral motion components that certainly contribute to additional underestimation of the real activity concentration present in lesions close to the diaphragm.

Respiratory gating of PET may improve the quantitative evaluation of lesions situated close to the diaphragm, because respiratory motion artifacts are significantly reduced. To reduce the underestimation attributable to this blurring effect, we used in this study only 1 of the 8 gates from each dynamic study. This approach has some limitations. Because only one-eighth of the information is retained in a single gated image, delineation of small nodules or lesions with low metabolic activity may become difficult, as noise increases at low count statistics. The signal-to-noise ratio may still improve with gating because of a reduction in the smearing of small nodules. It may be possible to use image morphing techniques to merge the 8 gated images into a single "fixed" image and recover lost counts. Another approach would be to sum selected gated frames throughout the gated acquisition, as respiratory motion occurs only during a fraction of each respiratory cycle.

In this study, only the emission acquisition was gated for respiration. It was not possible to gate the transmission scan on the scanner that we used because of hardware and software limitations. Because the transmission image used for attenuation correction was not gated, an "average" attenuation map was used to perform this correction on each gate throughout the respiratory cycle. As with CT-based attenuation correction for nongated PET images, an average transmission map induces artifacts on PET images obtained with respiratory gating. Optimal implementation of respiratory gating of PET data will require gating of the transmission data as well by use of conventional transmission scanning approaches with ^{68}Ge rod sources or ^{137}Cs single-point sources or by use of CT-based implementation.

Respiratory gating may be useful for combined PET/CT scanners, as the optimal method for obtaining CT images that are optimally coregistered with PET studies is still under debate. For diagnostic use, CT images are obtained preferably at the end of maximal inspiration, whereas PET images normally are obtained over the tidal volume. On average, PET images are closer to images obtained at the end of expiration. The main constraint of this situation arises from the acquisition times of these images, which varies from a few seconds for CT studies to a few minutes for PET scans. Breath holds are possible during a CT acquisition, but they are not feasible for the period of time necessary for a PET acquisition. This problem results in significant differences between the images obtained with these 2 methods, even when these acquisitions are performed just a few minutes apart in the same subject in the same position. The difficulty in coregistering the images can have 2 significant impacts: first, an inappropriate correction for attenuation is applied to PET images, and second, an inaccurate localization of abnormalities seen on PET can occur, as demonstrated recently in a study of clinically significant PET/CT artifacts (*28*). To minimize the difference, it was suggested that it would be preferable to obtain a CT scan at the end of normal expiration, as the position of the chest is closer to that observed in average PET acquisitions not corrected for respiratory motion (*29*,*30*). Another method for correcting the inevitable respiratory motion occurring during PET would be to use gated acquisition protocols to adjust the PET images to the CT data. Because respiratory motion is measured directly rather than modeled, PET data can be applied directly to a comparable CT acquisition, with reduced blurring and improved resolution in the chest and upper abdomen. With this intention, it was initially necessary to prove the feasibility of 3D whole-body PET acquisitions gated for respiration by use of a simple temperature-sensitive gating device. Other authors have used a more complex infrared camera tracking technique to correct for respiratory motion (*31*). Our method has the advantage of simplicity of design and implementation at a very low cost. With improved PET scanners that use fast scintillators, such as lutetium oxyorthosilicate and gadolinium oxyorthosilicate, higher peak-noise-equivalent count rates obtained in the 3D mode with standard ^{18}F-FDG doses may facilitate the use of gated approaches for correcting respiratory motion.

CONCLUSION

In this study, we have demonstrated the feasibility of routinely acquired respiratory motion-gated PET images of the thorax by use of ^{18}F-FDG with a low-cost device and standard gated acquisition software and without the need for hardware modification of a PET scanner or expensive motion tracking devices. Respiratory motion results in significant quantitative underestimation of uptake in small lung nodules at the base of the lungs. The detection of small lung nodules or small liver metastases might be improved by respiratory gating, and we intend to evaluate this method in a selected patient population. This approach also provides potential means for improving attenuation correction and image fusion with PET/CT devices, whether by gating the CT acquisition or by selecting gated PET data that optimally match CT data.

ACKNOWLEDGMENTS

The authors gratefully acknowledge the support of the SNM Education & Research Foundation (pilot study grant) and the Canadian Institutes for Health Research (clinician-scientist program).

REFERENCES

1. Pieterman RM, van Putten JW, Meuzelaar JJ, et al. Preoperative staging of non-small-cell lung cancer with positron-emission tomography. *N Engl J Med*. 2000;343:254–261.
2. Marom EM, Erasmus JJ, Patz EF. Lung cancer and positron emission tomography with fluorodeoxyglucose. *Lung Cancer*. 2000;28:187–202.
3. Lowe VJ, Duhaylongsod FG, Patz EF, et al. Pulmonary abnormalities and PET data analysis: a retrospective study. *Radiology*. 1997;202:435–439.
4. Weber WA, Ziegler SI, Thödtmann R, Hanauske AR, Schwaiger M. Reproducibility of metabolic measurements in malignant tumors using ^{18}F-FDG PET. *J Nucl Med*. 1999;40:1771–1777.
5. Kim CK, Gupta NC, Chandramouli B, Alavi A. Standardized uptake values of ^{18}F-FDG: body surface area correction is preferable to body weight correction. *J Nucl Med*. 1994;35:164–167.
6. Kim CK, Gupta NC. Dependency of standardized uptake values of fluorine-18 fluorodeoxyglucose on body size: comparison of body surface area correction and lean body mass correction. *Nucl Med Commun*. 1996;17:890–894.
7. Schomburg A, Bender H, Reichel C, et al. Standardized uptake values of fluorine-18 fluorodeoxyglucose: the value of different normalization procedures. *Eur J Nucl Med*. 1996;23:571–574.
8. Crippa F, Gavazzi C, Bozzetti F, et al. The influence of blood glucose levels on [^{18}F]fluorodeoxyglucose (FDG) uptake in cancer: a PET study in liver metastases from colorectal carcinomas. *Tumori*. 1997;83:748–752.
9. Diederichs CG, Staib L, Glatting G, Beger HG, Reske SN. ^{18}F-FDG PET: elevated plasma glucose reduces both uptake and detection rate of pancreatic malignancies. *J Nucl Med*. 1998;39:1030–1033.
10. Lowe VJ, DeLong DM, Hoffman JM, Coleman RE. Optimum scanning protocol for ^{18}F-FDG PET evaluation of pulmonary malignancy. *J Nucl Med*. 1995;36:883–887.
11. Kollins SA. Computed tomography of the pulmonary parenchyma and chest wall. *Radiol Clin North Am*. 1977;15:297–308.
12. Long FR, Castile RG, Brody AS, et al. Lungs in infants and young children: improved thin-section CT with a noninvasive controlled-ventilation technique—initial experience. *Radiology*. 1999;212:588–593.
13. Mori K, Saito Y, Tominaga K, et al. Three-dimensional computed tomography image of small pulmonary lesions. *Jpn J Clin Oncol*. 1992;22:159–163.
14. Wang Y, Riederer SJ, Ehman RL. Respiratory motion of the heart: kinematics and the implications for the spatial resolution in coronary imaging. *Magn Reson Med*. 1995;33:713–719.
15. van Geuns RJ, de Bruin HG, Rensing BJ, et al. Magnetic resonance imaging of the coronary arteries: clinical results from three dimensional evaluation of a respiratory gated technique. *Heart*. 1999;82:515–519.
16. Knopp MV, Bischoff HG. Evaluation of pulmonary lesions with positron emission tomography [in German]. *Radiologe*. 1994;34:588–591.
17. Hamacher K, Coenen HH, Stocklin G. Efficient stereospecific synthesis of no-carrier-added 2-[^{18}F]-fluoro-2-deoxy-D-glucose using aminopolyether supported nucleophilic substitution. *J Nucl Med*. 1986;27:235–238.
18. Cho K, Kumiata S, Okada S, Kumazaki T. Development of respiratory gated myocardial SPECT system. *J Nucl Cardiol*. 1999;6:20–28.
19. Robinson TE, Leung AN, Moss RB, Blankenberg FG, al-Dabbagh H, Northway WH. Standardized high-resolution CT of the lung using a spirometer-triggered electron beam CT scanner. *AJR*. 1999;172:1636–1638.
20. Kalender WA, Rienmuller R, Seissler W, Behr J, Welke M, Fichte H. Measurement of pulmonary parenchymal attenuation: use of spirometric gating with quantitative CT. *Radiology*. 1990;175:265–268.
21. Lemieux SK, Glover GH. An infrared device for monitoring the respiration of small rodents during magnetic resonance imaging. *J Magn Reson Imaging*. 1996;6:561–564.
22. Sugawara Y, Zasadny KR, Neuhoff AW, Wahl RL. Reevaluation of the standardized uptake value for FDG: variations with body weight and methods for correction. *Radiology*. 1999;213:521–525.
23. Keyes JW Jr. SUV: standard uptake or silly useless value? *J Nucl Med*. 1995;36:1836–1839.
24. Miyauchi T, Wahl RL. Regional 2-[^{18}F]fluoro-2-deoxy-D-glucose uptake varies in normal lung. *Eur J Nucl Med*. 1996;23:517–523.
25. Ter-Pogossian MM, Bergmann SR, Sobel BE. Influence of cardiac and respiratory motion on tomographic reconstructions of the heart: implications for quantitative nuclear cardiology. *J Comput Assist Tomogr*. 1982;6:1148–1155.
26. Mijailovich SM, Treppo S, Venegas JG. Effects of lung motion and tracer kinetics corrections on PET imaging of pulmonary function. *J Appl Physiol*. 1997;82:1154–1162.
27. Susskind H, Alderson PO, Dzebolo NN, et al. Effect of respiratory motion on pulmonary activity determinations by positron tomography in dogs. *Invest Radiol*. 1985;20:950–955.
28. Osman MM, Cohade C, Nakamoto Y, Marshall LT, Leal JP, Wahl RL. Clinically significant inaccurate localization of lesions with PET/CT: frequency in 300 patients. *J Nucl Med*. 2003;44:240–243.
29. Goerres GW, Kamel E, Heidelberg TN, Schwitter MR, Burger C, von Schulthess GK. PET-CT image co-registration in the thorax: influence of respiration. *Eur J Nucl Med Mol Imaging*. 2002;29:351–360.
30. Goerres GW, Burger C, Kamel E, et al. Respiration-induced attenuation artifact at PET/CT: technical considerations. *Radiology*. 2003;226:906–910.
31. Nehmeh SA, Erdi YE, Ling CC, et al. Effect of respiratory gating on quantifying PET images of lung cancer. *J Nucl Med*. 2002;43:876–881.